1521-0111/100/6/548–557$35.00
MOLECULAR PHARMACOLOGY

https://doi.org/10.1124/molpharm.121.000333
Mol Pharmacol 100:548–557, December 2021

Remdesivir and EIDD-1931 Interact with Human Equilibrative Nucleoside Transporters 1 and 2: Implications for Reaching SARS-CoV-2 Viral Sanctuary Sites[S]

Siennah R. Miller, Meghan E. McGrath, Kimberley M. Zorn, Sean Ekins, Stephen H. Wright, and Nathan J. Cherrington

College of Pharmacy, Department of Pharmacology & Toxicology (S.R.M., M.E.M., N.J.C.) and Department of Physiology (S.H.W.), University of Arizona, Tucson, Arizona; and Collaborations Pharmaceuticals, Inc., Raleigh, North Carolina (K.M.Z., S.E.)

Received June 7, 2021; accepted September 7, 2021

ABSTRACT

Equilibrative nucleoside transporters (ENTs) are present at the blood-testis barrier (BTB), where they can facilitate antiviral drug disposition to eliminate a sanctuary site for viruses detectable in semen. The purpose of this study was to investigate ENT-drug interactions with three nucleoside analogs, remdesivir, molnupiravir, and molnupiravir's active metabolite, β-D-N^4-hydroxycytidine (EIDD-1931), and four non-nucleoside molecules repurposed as antivirals for coronavirus disease 2019 (COVID-19). The study used three-dimensional pharmacophores for ENT1 and ENT2 substrates and inhibitors and Bayesian machine learning models to identify potential interactions with these transporters. In vitro transport experiments demonstrated that remdesivir was the most potent inhibitor of ENT-mediated [^{3}H]uridine uptake (ENT1 IC_{50}: 39 μM; ENT2 IC_{50}: 77 μM), followed by EIDD-1931 (ENT1 IC_{50}: 259 μM; ENT2 IC_{50}: 467 μM), whereas molnupiravir was a modest inhibitor (ENT1 IC_{50}: 701 μM; ENT2 IC_{50}: 851 μM). Other proposed antivirals failed to inhibit ENT-mediated [^{3}H]uridine uptake below 1 mM. Remdesivir accumulation decreased in the presence of 6-*S*-[(4-nitrophenyl)methyl]-6-thioinosine (NBMPR) by 30% in ENT1 cells ($P = 0.0248$) and 27% in ENT2 cells ($P = 0.0054$). EIDD-1931 accumulation decreased in the presence of NBMPR by 77% in ENT1 cells ($P = 0.0463$) and by 64% in ENT2 cells ($P = 0.0132$), which supported computational predictions that both are ENT substrates that may be important for efficacy against COVID-19. NBMPR failed to decrease molnupiravir uptake, suggesting that ENT interaction is likely inhibitory. Our combined computational and in vitro data can be used to identify additional ENT-drug interactions to improve our understanding of drugs that can circumvent the BTB.

SIGNIFICANCE STATEMENT

This study identified remdesivir and EIDD-1931 as substrates of equilibrative nucleoside transporters 1 and 2. This provides a potential mechanism for uptake of these drugs into cells and may be important for antiviral potential in the testes and other tissues expressing these transporters.

Introduction

The blood-testis barrier (BTB) protects developing germ cells, and some of the key components of this barrier are the tight junctions between the epithelial cells of the testis and efflux transporters present at the basal membrane of Sertoli cells (Mruk et al., 2011; Mruk and Cheng, 2015). The BTB can limit drug disposition and immune cell access to the male genital tract, creating an important sanctuary site where viruses can persist and potentially remain transmissible after drug treatment (Politch et al., 2012; Houzet et al., 2014; Soka et al., 2016; Uyeki et al., 2016; Deen et al., 2017; Robinson et al., 2018). Therapeutics that readily bypass this barrier may be more effective at treating viruses and inform the design and development of new antivirals that are able to reach sanctuary sites, such as the testes.

Equilibrative nucleoside transporter (ENT) 1 and ENT2 are ubiquitously expressed proteins that transport endogenous nucleosides across cell membranes. Due to similarity in chemical structure to endogenous ENT substrates, the ENTs are thought to transport nucleoside/nucleotide analogs. Recent studies have identified additional non-nucleoside analog antivirals, including darunavir and nevirapine, that interact with the ENTs (Miller et al., 2021a,b). Didanosine and ribavirin are two ENT substrates that are detectable in the semen of patients prescribed these drugs (Lowe et al., 2007;

This work was supported by National Institutes of Health National Institute of General Medical Sciences [Grants R01-GM123643 and R44-GM1 22196] and National Institutes of Health National Institute of Environmental Health Sciences [Grants P30-ES006694 and T32-ES007091-36A1].

S.E. is owner of Collaborations Pharmaceuticals Inc., and K.M.Z. is an employee. All other authors have no conflicts of interest.

https://dx.doi.org/10.1124/molpharm.121.000333.

[S] This article has supplemental material available at molpharm.aspetjournals.org.

ABBREVIATIONS: BTB, blood-testis barrier; COVID-19, coronavirus disease 2019; EIDD-1931, β-D-N^4-hydroxycytidine; ENT, equilibrative nucleoside transporter; K_t, concentration to reach half-maximal rate of transport; LC-MS/MS, liquid chromatography with tandem mass spectrometry; NBMPR, 6-*S*-[(4-nitrophenyl)methyl]-6-thioinosine; OATP, organic anion–transporting polypeptide; SARS-CoV-2, severe acute respiratory syndrome coronavirus 2; WB, Waymouth's buffer.

Hofer et al., 2010). The transepithelial transport pathway that is created by ENT1 on the basal membrane of Sertoli cells and ENT2 on the apical membrane of Sertoli cells provides a mechanism for antivirals that are substrates of these transporters to cross the BTB (Klein et al., 2013).

Repurposing molecules as broad-spectrum antivirals has the potential to bypass drug discovery and development, enabling these compounds to reach patients quicker. Computational and in vitro approaches implemented early in the research and development process can also reduce the likelihood of undesirable off-target effects later in the process (Kola and Landis, 2004; Bowes et al., 2012). Remdesivir is a nucleoside analog that was initially developed to treat hepatitis C virus. It was subsequently repurposed to treat Ebola virus and has since demonstrated activity against other RNA viruses, including severe acute respiratory syndrome coronavirus 2 (SARS-CoV-2) (Siegel et al., 2017; Mulangu et al., 2019; Eastman et al., 2020), for which it is US Food and Drug Administration–approved. Molnupiravir is currently being evaluated for the treatment of coronavirus disease 2019 (COVID-19) (Cox et al., 2021; National Clinical Trial 04405739). Additionally, there is continued interest in exploring other known inhibitors of the Ebola virus, including tilorone, pyronaridine, quinacrine, and, controversially, hydroxychloroquine (Sagara et al., 2018; Ekins et al., 2018, 2019, 2020; Lane et al., 2019; Baker et al., 2020; Ekins and Madrid, 2020; Lane et al., 2020a,b; Lane and Ekins, 2020; Naghipour et al., 2020; Bailly, 2021; Puhl et al., 2021), as potential treatments for COVID-19. SARS-CoV-2 is detectable in the semen of patients (Li et al., 2020). Ebola virus is also sexually transmitted (Malvy et al., 2019); therefore, it is essential that treatments for this virus and other sexually transmitted viruses (e.g., human immunodeficiency virus) are able to reach the site of transmission. There are monoclonal antibody treatments for Ebola virus, but none are small-molecule treatments approved to date (Kaplon and Reichert, 2021; Markham, 2021) or specifically focused on reaching the virus sanctuary sites.

The purpose of this study was to investigate interactions of the antiviral drugs remdesivir, tilorone, pyronaridine, quinacrine, hydroxychloroquine, molnupiravir, and molnupiravir's active metabolite, β-D-N^4-Hydroxycytidine (EIDD-1931), with ENT1 and ENT2. Interactions were investigated using computational approaches and results were validated using previously established in vitro methods to identify substrates and inhibitors of the ENTs (Miller et al., 2021a,b). The computational methods and transport experiments were completed in an exploratory manner. Identifying drugs that are both effective in treating sexually transmitted viruses and are substrates of the ENTs could be useful to identify drugs to prevent further sexual transmission, prevent viral relapse after treatment, and elucidate the broader roles of these transporters in drug disposition.

Materials and Methods

Reagents. [^{3}H]Uridine (specific activity 35.8 Ci/mmol) and MicroScint-20 scintillation cocktail were purchased from PerkinElmer (Waltham, MA). Remdesivir, molnupiravir, EIDD-1931, cladribine, tilorone, and quinacrine were purchased from Cayman Chemical (Ann Arbor, MI). Pyronaridine tetraphosphate [4-[(7-chloro-2-methoxybenzo[b][1,5]naphthyridin-10-yl)amino]-2,6-bis(1-pyrrolidinylmethyl)phenol phosphate (1:4)] was purchased from BOC Sciences (Shirley, NY). The purity of these compounds is greater than 95%. Hydroxychloroquine was purchased from Sigma-Aldrich (St. Louis, MO). 6-*S*-[(4-Nitrophenyl)methyl]-6-thioinosine (NBMPR) was purchased from Tocris Bioscience (Bristol, UK). Poly(L-lysine) (10 mg/ml) was purchased from ScienCell (Carlsbad, CA). Additional reagents were purchased from Thermo Fisher Scientific (Waltham, MA).

Ligand-Based Substrate and Inhibitor Pharmacophores. Three-dimensional quantitative structure activity relationship pharmacophores previously generated for ENT1 and ENT2 using Discovery Studio (Biovia; San Diego, CA) were used to score transporter interactions with the antivirals in this study (Miller et al., 2021a). For pharmacophores, known substrates with reported K_t (concentration to reach half-maximal rate of transport) values were used to measure biologic activity, and IC_{50} values were used as a measure of biologic activity for inhibitor pharmacophores. Hydrogen bond acceptor, hydrogen bond donor, and hydrophobic positive and negative ionizable features were selected for pharmacophore generation. A more detailed description on ENT ligand–based pharmacophore generation has been previously provided (Miller et al., 2021a). Mapping of compounds to ligand-based pharmacophores was completed in an exploratory manner.

Assay Central Bayesian Models. Assay Central Bayesian models were generated using a ChEMBL training set containing ENT1 IC_{50} values that was previously described and data curated from the literature (Miller et al., 2021a,b). These models were generated to predict ENT1 activity from chemical structures. The ChEMBL training set used was Target ID 1997 (https://www.ebi.ac.uk/chembl/target_report_card/CHEMBL1997). Active compounds are predicted to interact with the ENTs, whereas inactive compounds are predicted to not interact with the ENTs. Thresholds for actives/inactives were 2 μM for the ChEMBL model, 316 mM for the model generated using previously published data by our group, 0.66 μM for the ENT1 model using literature data, and 13 μM for the ENT2 model using literature data (Miller et al., 2021a,b). These Bayesian models were used to generate prediction and applicability scores that predict the activity of remdesivir, tilorone, pyronaridine, quinacrine, hydroxychloroquine, and molnupiravir. Further details on the ENT Assay Central Bayesian models can be found in earlier publications (Sandoval et al., 2018; Miller et al., 2021a,b). Prediction and applicability scores for each compound were completed in an exploratory manner.

Cell Culture. HeLa ENT cells that functionally express either ENT1 or ENT2 were generated from wild-type HeLa S3 CCL-2.2 cells using CRISPR/Cas9 and were maintained according to the same culturing protocol for wild-type HeLa S3 CCL-2.2 cells provided by American Type Culture Collection (Manassas, VA) (Miller et al., 2021a,b). ENT cells were grown in Ham's F12K medium containing 1.5 g/l sodium bicarbonate, 1% v/v penicillin/streptomycin, and 10% v/v fetal bovine serum. Cells were kept at 37°C in a humidified 5% CO_2 incubator. Cells were routinely tested for potential mycoplasma contamination. ENT1 and ENT2 cells were characterized in a previous publication (Miller et al., 2021b). In ENT1 cells, functional loss of ENT2 is a result of a deletion in exon 1. In ENT2 cells, functional loss of ENT1 is a result of a deletion in exon 5 (Miller et al., 2021b). One hundred nanomolar NBMPR eliminates [^{3}H]uridine uptake in ENT1 cells, and 100 μM NBMPR eliminates [^{3}H]uridine in ENT2 cells (Miller et al., 2021b).

Transport Experiments. Experiments were performed as described previously (Miller et al., 2021a,b) except HeLa ENT cells were seeded 1 day prior to experiments in poly(L-lysine)–coated 96-well plates at 35,000 cells/well. All experiments were conducted with confluent cell monolayers at room temperature (n = 3). Transport buffers were made in Waymouth's Buffer (WB; 2.5 mM $CaCl{\bullet}2H_2O$, 28 mM D-glucose, 13 mM HEPES, 135 mM NaCl, 1.2 mM $MgCl_2$, 0.8 mM $MgSO_4{\bullet}7H_2O$, pH 7.4). Fresh transport buffer solutions were prepared for each experiment. All transport experiments were completed in an exploratory manner. Remdesivir stocks were prepared

in 100% DMSO and carefully diluted into transport buffer with a final concentration of 2% v/v DMSO. Preliminary studies established that 2% v/v DMSO in transport buffer does not interfere with transport experiments in these cells. Cells were washed twice with WB, and then 50 μl of transport buffer containing 1 μCi/ml (~30 nM) [^{3}H]uridine and increasing concentrations of antiviral drug was added to cells. Transport was terminated after 5 minutes by rinsing cells three times with WB. Two hundred microliters of liquid scintillation cocktail was added to cells before determining the total accumulated radioactivity using a liquid scintillation counter. Transport experiments were completed in an exploratory manner. For transport experiments with liquid chromatography with tandem mass spectrometry (LC-MS/MS), no [^{3}H]uridine was included in the transport buffer. Based on the calculated IC_{50} values for remdesivir, molnupiravir, and EIDD-1931, 50 μM remdesivir was used for remdesivir accumulation experiments, 500 μM molnupiravir was used for molnupiravir accumulation experiments, and 250 μM EIDD-1931 was used for EIDD-1931 accumulation experiments. After terminating transport, samples were prepared for LC-MS/MS by adding 50 μl of 1:1 methanol:acetonitrile to cells containing 100 ng/ml of internal standard (cladribine) and incubated overnight at 4°C (Miller et al., 2021a,b). Calibration curves were prepared identically to samples. Remdesivir and molnupiravir samples were dried and resuspended in 50 μl of 90:10 H_2O:acetonitrile + 0.1% formic acid.

LC-MS/MS Detection and Quantification. A Shimadzu Prominence HPLC system (Kyoto, Japan) coupled to a SCIEX QTRAP 4500 mass spectrometer (Framingham, MA) was used. Ten microliters of sample was injected onto an Agilent Poroshell 120 C18 column (Santa Clara, CA). Supplemental Table 2 contains multiple reaction monitoring transitions and instrumental parameters. Separate methods were developed and used for the detection of remdesivir and molnupiravir. Remdesivir and molnupiravir were detected in positive ion mode and separated over a binary gradient of water with 0.1% formic acid (A) and acetonitrile with 0.1% formic acid (B) at a flow rate of 0.3 ml/min. For remdesivir, it proceeded as 10% B (0–1 minutes), 10% to 90% B (1–3 minutes), 90% B (3–4 minutes), 90% to 10% B (4–4.5 minutes), and 10% B (4.5–6 minutes). For molnupiravir, it proceeded as 10% B (0–1 minutes), 10% to 90% B (1–3 minutes), 90% B (3–4 minutes), 90% to 10% B (4–4.5 minutes), and 10% B (4.5–6 minutes). The column was equilibrated with 10% B for 0.5 minutes between remdesivir and molnupiravir samples. EIDD-1931 was detected in positive ion mode and separated over a binary gradient of water with 0.1% formic acid (A) and acetonitrile with 0.1% formic acid (B) at a flow rate of 0.4 ml/min. For EIDD-1931, it proceeded as 2.5% B (0–1 minutes), 2.5% to 90% B (1–4 minutes), 90% B (4–4.5 minutes), and 90% to 10% B (4.5–5 minutes). The column was equilibrated with 2.5% B for 2 minutes between EIDD-1931 samples. Data were analyzed using MultiQuant MD 3.0.2 (SCIEX; Framingham, MA) before statistical analysis was completed using GraphPad Prism version 9.0 (San Diego, CA).

Data Analysis. All transport experiments were done in duplicate using three separate cell passages ($n = 3$). Data from LC-MS/MS transport experiments were converted from nanograms per milliliter to picomole per negative square centimeters (nominal cell surface area). Data are reported as mean and standard deviation. The IC_{50} value of remdesivir, tilorone, pyronaridine, quinacrine, and hydroxychloroquine on ENT1- and ENT2-mediated [^{3}H]uridine uptake was calculated using eq. 1 for each individual experiment (Miller et al., 2021a,b).

$$J = \left[\left(J_{app-max} * T\right)/\left(IC_{50} + [S]\right)\right] + \left(K_d * T\right) \quad \text{(Eq. 1)}$$

In eq. 1, J is total uridine transport, $J_{app-max}$ is a constant (J_{max} times the ratio of the IC_{50} for the antiviral and the K_t for uridine), T is [^{3}H]uridine concentration, and S is antiviral concentration. To compare ENT1 and ENT2 IC_{50} values for each experiment, an unpaired t test ($P \leq 0.05$) was used. Antiviral uptake studies in the presence and absence of NBMPR were compared using an unpaired, two-tailed t test ($P \leq 0.05$). Because of the exploratory nature of experiments, the outcomes of all statistical tests are descriptive. Means and statistical tests were based on technical replicates.

Results

Ligand-Based Substrate and Inhibitor Pharmacophores. Table 1 reports fit values and estimated K_t and IC_{50} values for antivirals mapped to the ENT substrate and inhibitor pharmacophores. Remdesivir had the highest fit value to the ENT1 and ENT2 substrate pharmacophores (Fig. 1, A and D). Additionally, remdesivir had the highest fit value for both ENT1 and ENT2 inhibitor pharmacophores (Fig. 2, A and D). Molnupiravir also had high fit values to the ENT substrate and inhibitor pharmacophores (Figs. 1, B and E, and 2, B and E). Remdesivir had the lowest estimated K_t values for ENT1 and ENT2 (Table 1).

Assay Central Bayesian Models. Bayesian models were generated using the ENT1 inhibitor dataset from ChEMBL, previously published data from our laboratory, and data curated from literature searches on ENT1 and ENT2 interactions (Miller et al., 2021a,b). Each model had different automatically calculated thresholds to consider a compound as active or inactive. Although these vary, the receiver operating characteristic values are very good (i.e., >0.8), whereas the two binary dataset receiver operating characteristic values (Fig. 3, B and C) are acceptable (approximately 0.71), likely a product of their smaller size in comparison with the

TABLE 1
Estimated K_t values and fit values for compounds mapped to the ENT substrate pharmacophores and estimated IC_{50} values and fit values for compounds mapped to the ENT inhibitor pharmacophores

ENT1 Substrate	Estimate K_t (μM)	Fit Value
Remdesivir	2	6.41
Molnupiravir	32	5.26
EIDD-1931	1	6.61
Hydroxychloroquine	147	4.61
ENT2 Substrate	**Estimate K_t (μM)**	**Fit Value**
Remdesivir	41	6.22
Molnupiravir	74	5.96
EIDD-1931	76	5.95
Hydroxychloroquine	4,424	4.19
Pyronaridine	13,624	3.70
Quinacrine	19,091	3.56
Tilorone	550,687	2.09
ENT1 Inhibitor	**Estimate IC_{50} (μM)**	**Fit Value**
Remdesivir	0.06	8.71
Molnupiravir	4	6.85
EIDD-1931	70	5.66
Hydroxychloroquine	632	4.71
Pyronaridine	635	4.70
Quinacrine	633	4.70
Tilorone	632	4.71
ENT2 Inhibitor	**Estimate IC_{50} (μM)**	**Fit Value**
Remdesivir	9	5.82
Molnupiravir	7	5.75
EIDD-1931	53	4.95
Hydroxychloroquine	368	4.11
Pyronaridine	411	4.07
Quinacrine	416	4.06
Tilorone	368	4.11

Tilorone, quinacrine, and pyronaridine were not predicted to map to the ENT1 substrate pharmacophore.

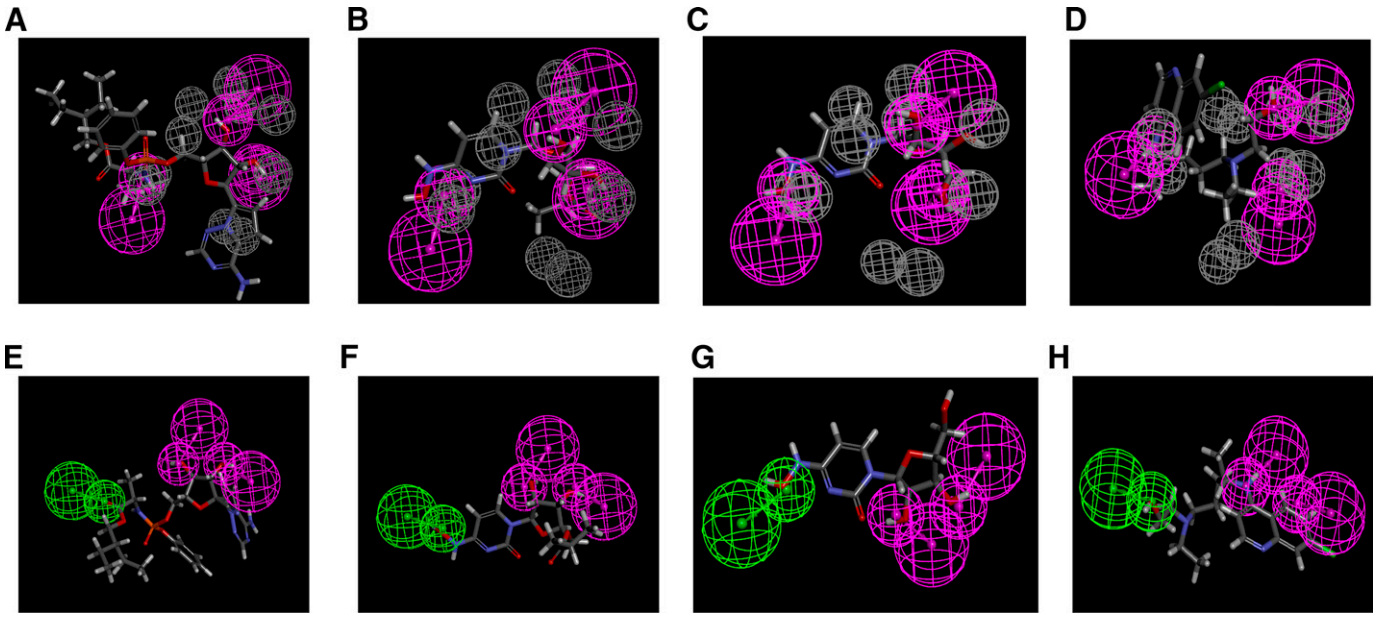

Fig. 1. ENT1 and ENT2 substrate pharmacophores. ENT1 substrate pharmacophore with (A) remdesivir, (B) molnupiravir, (C) EIDD-1931, and (D) hydroxychloroquine mapped and ENT2 substrate pharmacophore with (E) remdesivir, (F) molnupiravir, (G) EIDD-1931, and (H) hydroxychloroquine mapped. Gray represents excluded volumes, and purple represents hydrogen bond donors.

others. The calculated thresholds, however, produce a ratio of actives to inactives that is encouraging, especially as Bayesian algorithms have been shown to be well suited to handle unbalanced datasets in our various earlier studies (Clark et al., 2015; Clark and Ekins, 2015). Prediction scores ≥0.5 designated a compound as active. Prediction and applicability scores for remdesivir, molnupiravir, tilorone, pyronaridine, quinacrine, and hydroxychloroquine are included in Supplemental Table 1.

Inhibitory Interactions with ENT1 and ENT2. The IC_{50} values of remdesivir, molnupiravir, EIDD-1931, tilorone, pyronaridine, quinacrine, and hydroxychloroquine on ENT1- and ENT2-mediated [^{3}H]uridine uptake were calculated using eq. 1 and reported in Table 2 and plotted in Fig. 4. Remdesivir was the most potent inhibitor of both ENT1 (IC_{50}: 38 ± 2 μM) and ENT2 (IC_{50}: 73 ± 14 μM), and calculated IC_{50} values were different for ENT1 and ENT2 (P = 0.0106). EIDD-1931 was the second-most potent inhibitor of both transporters (ENT1 IC_{50}: 259 ± 118 μM; ENT2 IC_{50}: 467 ± 101 μM), and calculated IC_{50} values were similar (P = 0.0806). Molunpiravir was the third-most potent inhibitor of both transporters (ENT1 IC_{50}: 701 ± 294 μM; ENT2 IC_{50}: 851 ± 152 μM), and calculated IC_{50} values were similar for ENT1 and ENT2 (P = 0.4749). Tilorone, pyronaridine, quinacrine, and hydroxychloroquine did not inhibit ENT1- or ENT2-mediated [^{3}H]uridine uptake well; calculated IC_{50} values were greater than 900 μM, with most being greater than 2 mM. There was no difference in calculated IC_{50} values for tilorone (P = 0.1063), quinacrine (P = 0.1377), or hydroxychloroquine (P = 0.3847);

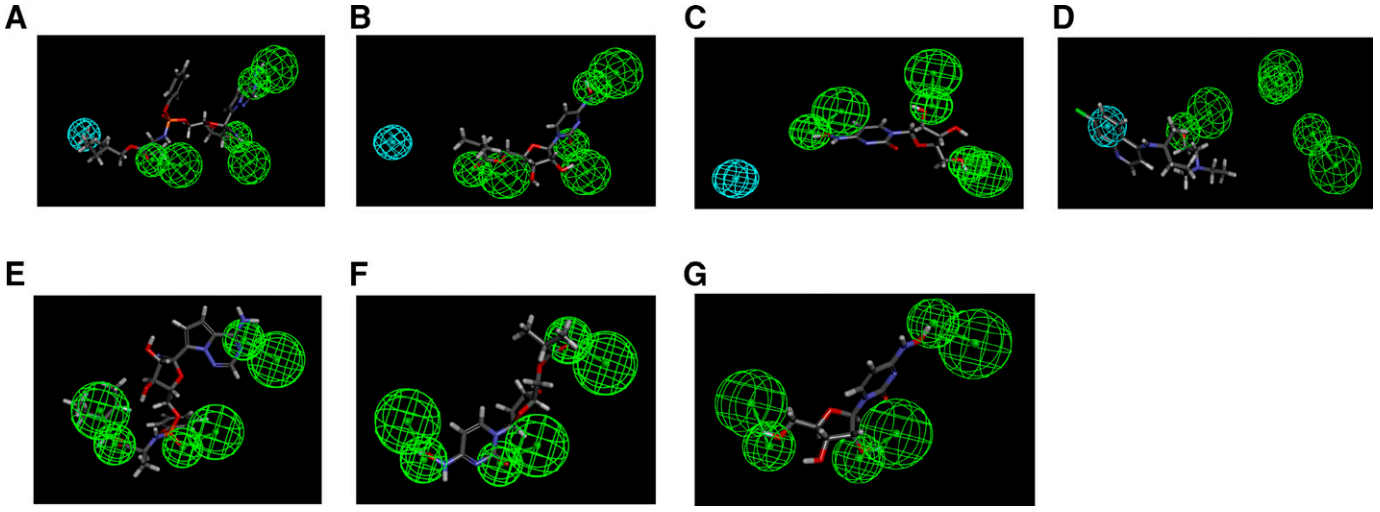

Fig. 2. ENT1 and ENT2 inhibitor pharmacophores. ENT1 inhibitor pharmacophore with (A) remdesivir, (B) molnupiravir, (C) EIDD-1931, and (D) hydroxychloroquine mapped and ENT2 inhibitor pharmacophore with (E) remdesivir, (F) molnupiravir, and (G) EIDD-1931 mapped. Gray represents excluded volumes, cyan represents hydrophobic groups, and green represents hydrogen bond acceptors.

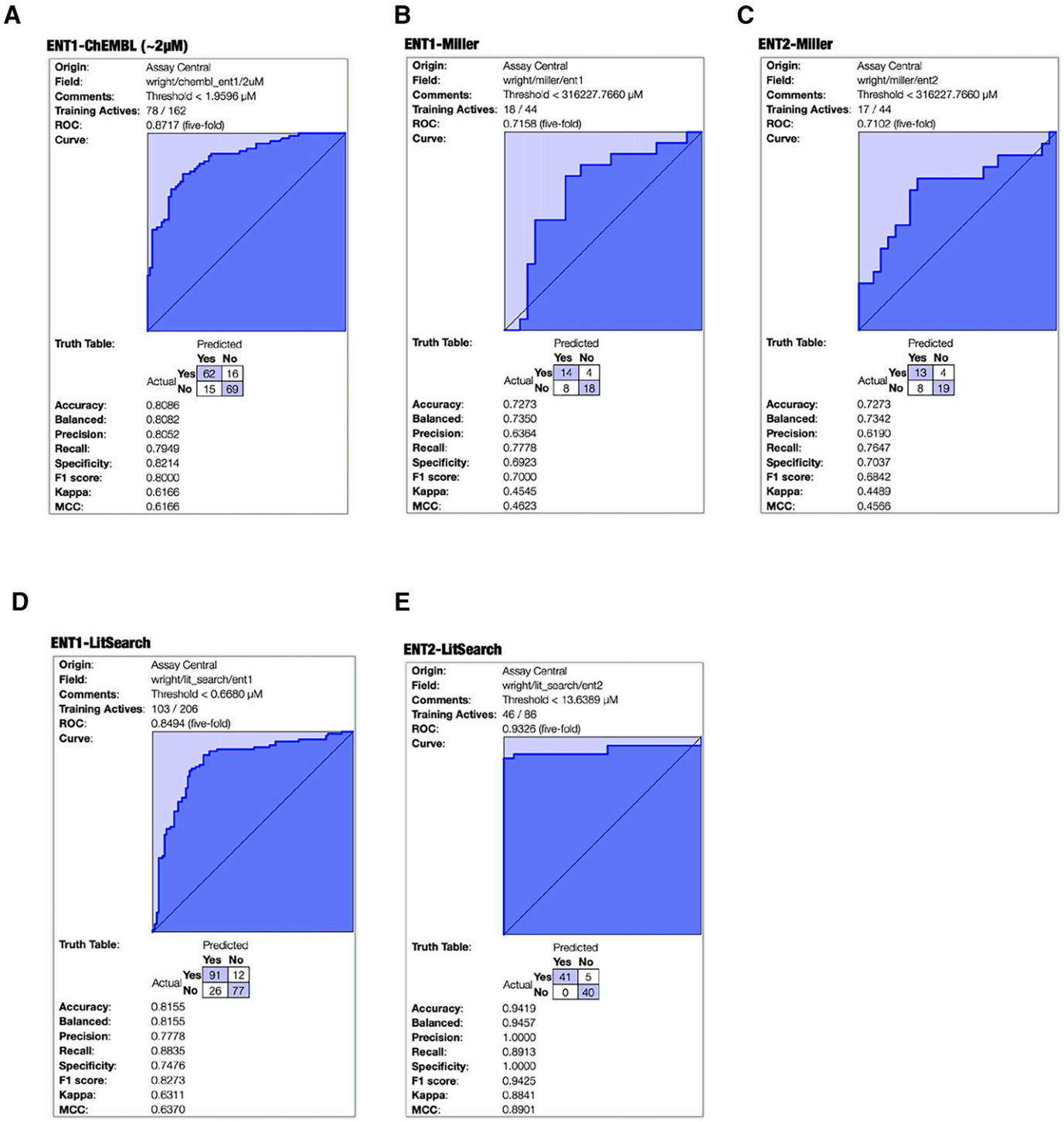

Fig. 3. Updated Bayesian models integrating established models for ENTs with compounds used in this study. (A) ENT1-ChEMBL model (Miller et al., 2021b), (B) ENT1 model using data from our laboratory (Miller et al., 2021b), (C) ENT2 model using data from our laboratory (Miller et al., 2021b), (D) ENT1 model using literature data (Miller et al., 2021a), and (E) ENT2 model using literature data (Miller et al., 2021a). MCC, Matthews correlation coefficient; ROC, receiver operating characteristic.

however, there was a difference in calculated IC_{50} values for pyronaridine ($P = 0.0052$).

Remdesivir, Molnupiravir, and EIDD-1931 Transport. The accumulation of remdesivir and molnupiravir in ENT1 and ENT2 cells in the presence and absence of 100 μM NBMPR was determined. Remdesivir accumulation decreased in the presence of NBMPR by 30% in ENT1 cells (90.4 ± 6.42 vs. 63.9 ± 11.4 pmol cm^{-2} remdesivir; $P = 0.0248$) and by 27% in ENT2 cells (103 ± 8.25 vs. 75.9 ± 2.80 pmol cm^{-2} remdesivir; $P = 0.0054$). Molnupiravir accumulation did not decrease in the presence of NBMPR in ENT1 cells (30.4 ± 2.10 vs. 31.7 ± 5.77 pmol cm^{-2} molnupiravir; $P = 0.7248$) or ENT2

TABLE 2
Calculated antiviral IC_{50} values for ENT1- and ENT2-mediated [^{3}H]uridine uptake

Antiviral	ENT1 IC_{50} μM ± S.D.	ENT1 −Log (IC_{50}) ± −Log (S.D.)	ENT2 IC_{50} μM ± S.D.	ENT2 −Log (IC_{50}) ± −Log (S.D.)
Remdesivir	39 ± 2	−1.6 ± −0.3	77 ± 14	−1.9 ± −1.1
Molnupiravir	701 ± 294	−2.8 ± −2.5	851 ± 152	−2.9 ± −2.2
EIDD-1931	259 ± 118	−2.4 ± −2.1	467 ± 101	−2.7 ± −2.0
Quinacrine	8494 ± 7022	−3.9 ± −3.8	950 ± 695	−3.0 ± −2.8
Tilorone	6256 ± 2173	−3.8 ± −3.3	2943 ± 1704	−3.5 ± −3.2
Hydroxychloroquine	9186 ± 6347	−4.0 ± −3.8	269,961 ± 463,122	−5.4 ± −5.6
Pyronaridine	13676 ± 3612	−4.1 ± −3.6	1548 ± 1185	−3.2 ± −3.1

Data are presented as mean and S.D. and −Log mean and S.D.

cells (32.1 ± 3.90 vs. 31.8 ± 5.90 pmol cm^{-2} molnupiravir; P = 0.9431). EIDD-1931 accumulation decreased in the presence of NBMPR by 77% in ENT1 cells (90.6 ± 41.8 vs. 20.9 ± 6.70 pmol cm^{-2}EIDD-1931; P = 0.0463) and by 64% in ENT2 cells (74.1 ± 13.4 vs. 26.8 ± 13.8 pmol cm^{-2} EIDD-1931; P = 0.0132).

Discussion

We have shown for the first time that remdesivir and EIDD-1931 are substrates of ENT1 and ENT2, which have implications for reaching SARS-CoV-2 viral sanctuary sites. The transepithelial transport pathway created by ENT1 and ENT2 in Sertoli cells provides a potential entry mechanism for antivirals to cross the BTB, potentially eliminating this viral sanctuary site (Klein et al., 2013; Miller and Cherrington, 2018). Antivirals that are transported by the ENTs not only have the ability to cross the BTB but also penetrate other tissues since these transporters are widely expressed in the human body (Pennycooke et al., 2001; Molina-Arcas et al., 2009). This study therefore used a combination of computational (pharmacophores and Bayesian models) and in vitro approaches to determine whether seven antivirals with activity against SARS-CoV-2 (and other viruses) interacted with ENT1 and ENT2. The value of computational approaches to identify drug-transporter interactions was demonstrated through earlier studies (Miller et al., 2021a,b) and here with remdesivir and molnupiravir.

Remdesivir was computationally predicted to be the most potent inhibitor of ENT1 and ENT2 and a substrate of both transporters. Metabolites of remdesivir were not investigated because remdesivir needs to enter cells before intracellular conversion occurs, and the purpose of our study was to explore the roles of the ENTs in remdesivir uptake. We determined the IC_{50} values for seven antivirals on ENT1- and ENT2-mediated [^{3}H]uridine uptake and measured remdesivir uptake in the presence of the ENT-specific inhibitor, NBMPR. Remdesivir was estimated to inhibit ENT1 in the low-nanomolar range and ENT2 in the low-micromolar range. Our studies determined that remdesivir inhibited ENT1- and ENT2-mediated [^{3}H]uridine uptake in the low-micromolar range. EIDD-1931 was estimated to inhibit ENT1 and ENT2 in the low-micromolar range, and our studies determined that EIDD-1931 inhibited ENT1- and ENT2-mediated [^{3}H]uridine uptake in the mid-micromolar range. Additional experiments showed that remdesivir and EIDD-1931 are substrates of ENT1 and ENT2 (Fig. 5, A, B, E, and F).

The experimentally determined IC_{50} values for remdesivir were slightly higher than the estimated K_t values (estimated K_t ENT1: 2 μM and ENT2: 41 μM). The inhibition profile of remdesivir and EIDD-1931 on ENT-mediated [^{3}H]uridine uptake aligns with IC_{50} values for other known substrates, including endogenous nucleosides and nucleoside analog drugs (Miller et al., 2021b). These data align with Bayesian model predictions at higher thresholds. The experimentally determined IC_{50} values of molnupiravir were also higher than estimated IC_{50} values, and subsequent data suggested that molnupiravir's interaction with the ENTs is limited to inhibition (Fig. 5, C and D). The experimentally determined IC_{50} values of EIDD-1931 were higher than estimated K_t values (estimated K_t ENT1: 1.5 μM and ENT2: 76 μM). Tilorone, pyronaridine, quinacrine, and hydroxychloroquine did not interact effectively with either of the ENTs, as predicted with pharmacophores (although not by Bayesian models). Overall, our computational predictions of ENT-drug interactions generally aligned with our in vitro data.

Remdesivir is currently used for the treatment of hospitalized patients with COVID-19 (Eastman et al., 2020; Gilead Sciences, 2020; Jorgensen et al., 2020). Once remdesivir enters cells, it is converted to its active metabolite by kinases (Gilead Sciences, 2020). It is a known substrate of organic anion–transporting polypeptide (OATP) 1B1 and P-glycoprotein and also interacts with OATP1B3 and OATP2B1 (Gilead Sciences, 2020; Nies et al., 2021; Telbisz et al., 2021). Remdesivir inhibited OATP1A2 and OATP2B1 in the low-micromolar range (~4 μM) (Telbisz et al., 2021). Nies et al. (2021) concluded that although remdesivir is a substrate of OATP1B1, low uptake rates suggest that OATP1B1 is not important for uptake into hepatocytes. The identification of remdesivir as a substrate of ENT1 and ENT2 provides a potentially viable mechanism for remdesivir uptake into cells. The list of transporters recommended for the investigation of potential unwanted drug-drug interactions (U.S. Department of Health and Human Services, 2020) does not currently include either ENT1 or ENT2. The reported maximum plasma concentrations of remdesivir is ~7.3 μM after a single dose, and ~3.7 μM after multiple doses (Gilead Sciences, 2020; Humeniuk et al., 2021). High plasma protein binding indicate there is a low potential for remdesivir to interact with these transporters in vivo due to lower unbound drug concentrations. However, the presence of a carrier-mediated pathway does provide a mechanism for remdesivir to cross the plasma membrane. Molnupiravir is also currently in clinical trials for the treatment of COVID-19 (Cox et al., 2021; Wahl et al., 2021; National Library of Medicine National Clinical Trial, 2020), and to date, there is no published information on molnupiravir-transporter interactions. Molnupiravir is hydrolyzed to its active metabolite, EIDD-1931, which

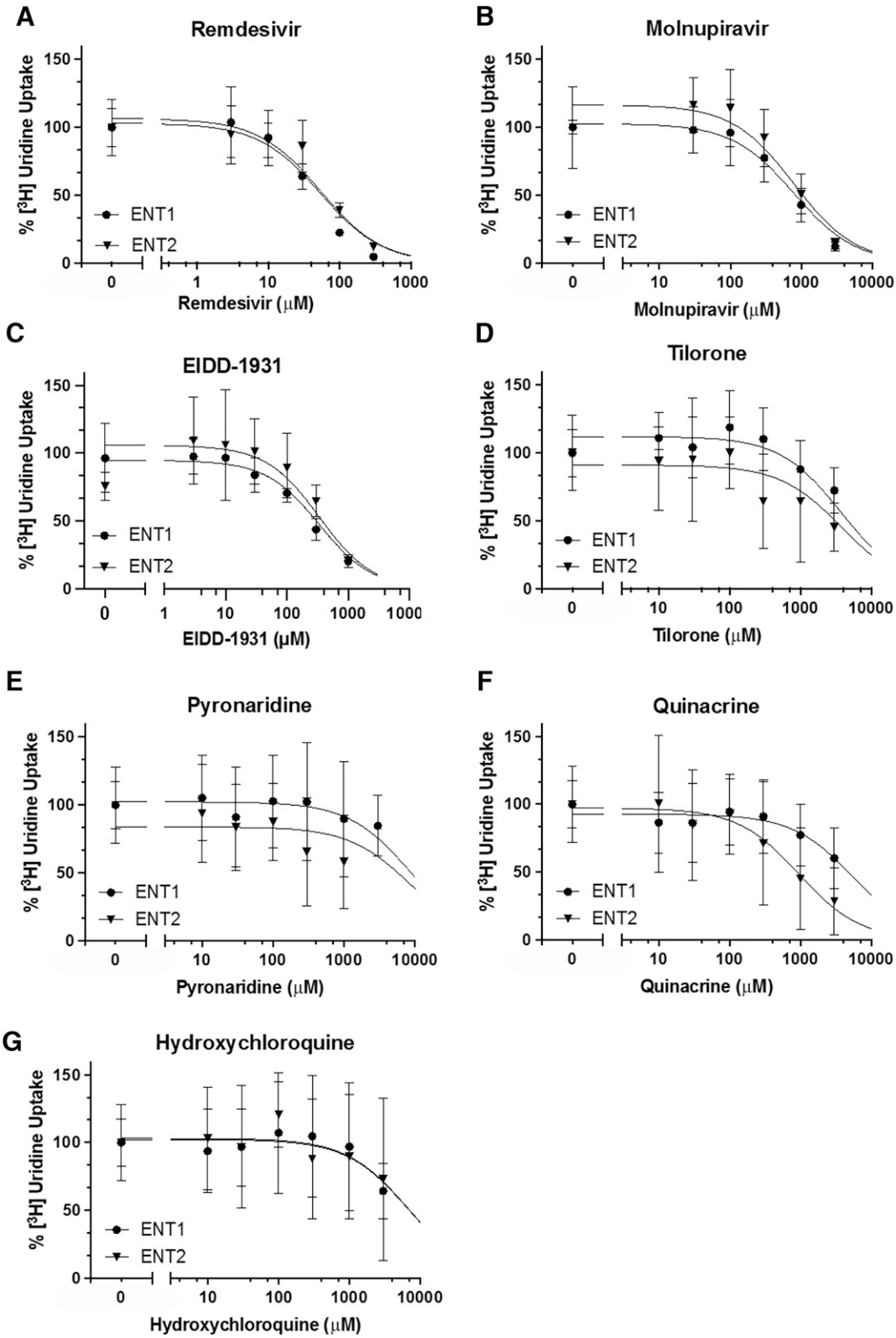

Fig. 4. Antiviral Inhibition of ENTs. Inhibition of ENT1- and ENT2-mediated [^{3}H]uridine uptake by (A) remdesivir, (B) molnupiravir, (C) EIDD-1931, (D) tilorone, (E) pyronaridine, (F) quinacrine, and (G) hydroxychloroquine. Data are presented as mean ± S.D., $n = 3$. Calculated IC_{50} values are reported in Table 2.

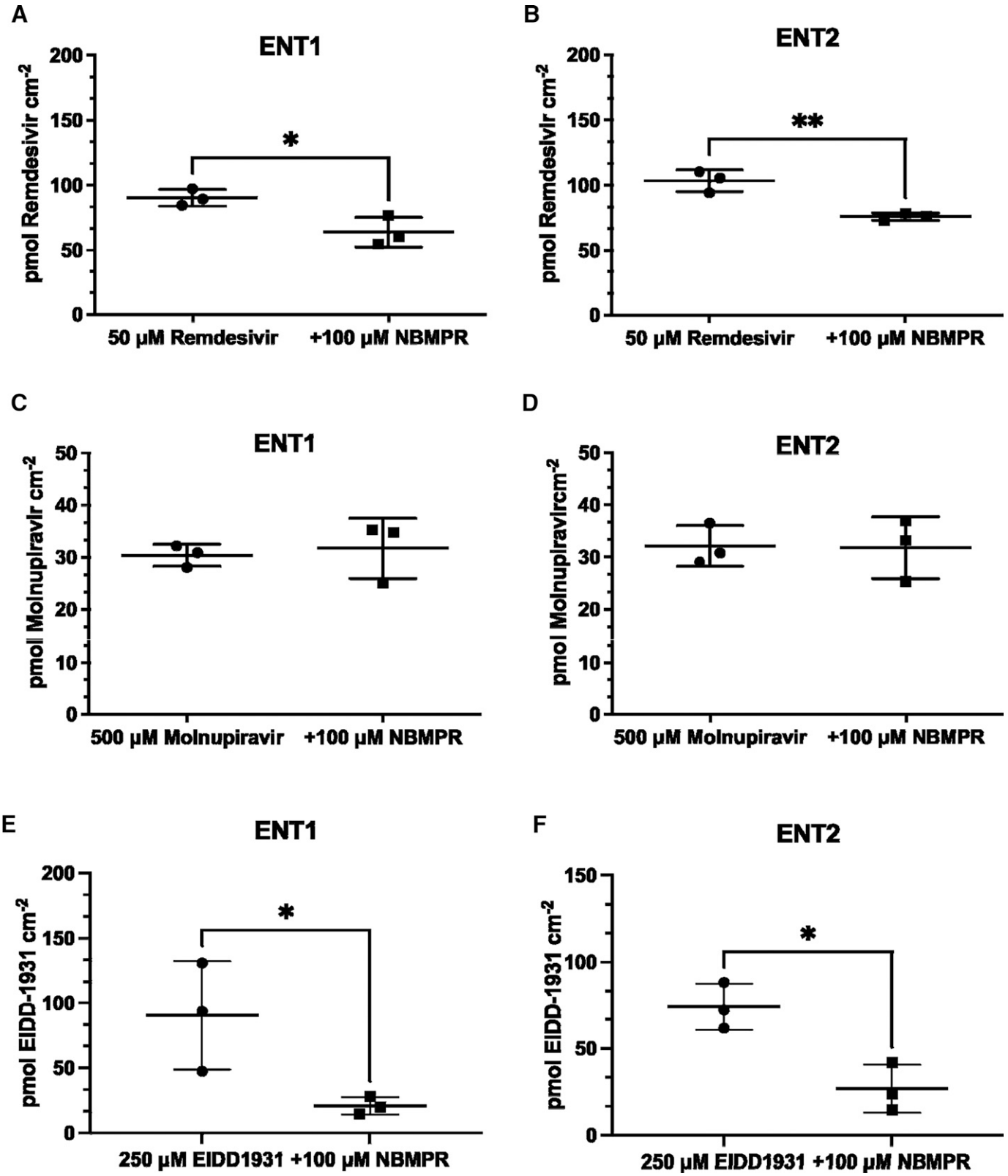

Fig. 5. Antiviral uptake in ENT1 and ENT2 cell lines. Remdesivir (50 µM) uptake in ENT1 (A) and ENT2 (B) cell lines. Molnupiravir (500 µM) uptake in ENT1 (C) and ENT2 (D) cell lines. EIDD-1931 (250 µM) uptake in ENT1 (E) and ENT2 (F) cell lines. All experiments were terminated after 5 minutes. Data are presented as mean ± S.D., $n = 3$. A two-tailed, unpaired t test was used to determine the difference between groups with $^*P \leq 0.05$.

currently has no known documented transporter interactions. The reported maximum plasma concentration of EIDD-1931 after a single-dose study of molnupiravir was ~24.5 μM and was achieved with a 1600-mg dose molnupiravir (Painter et al., 2021). Drug potency for ENTs cannot be solely interpreted based on determined in vitro IC_{50} values and should be seen relative to expected exposure levels. In this study, we determined that EIDD-1931 but not molnupiravir is a substrate of ENT1 and ENT2. The identification of EIDD-1931 as a substrate provides a potential mechanism for EIDD-1931 uptake into cells, may be important for antiviral potential in the testes, and may potentially reduce sexual transmission of viruses.

This study is the first to demonstrate that ENT1 and ENT2 contribute to the cellular uptake of remdesivir and EIDD-1931 in vitro and may also define a key mechanistic difference in the ability of these specific therapeutics to directly reach viral sanctuary sites. The ENT transporters may similarly play a role in cellular remdesivir uptake in humans. Generation of additional data like this study will allow us to improve and update the computational models used in this study to identify drug interactions with the ENTs. Information from these models can also inform and facilitate the development of additional broad-spectrum antivirals that may be useful for other viruses like human immunodeficiency virus, Zika, and Ebola to address potential viral sanctuary sites.

Authorship Contributions

Participated in research design: Miller, McGrath, Zorn, Ekins, Wright, Cherrington.

Conducted experiments: Miller, McGrath, Zorn, Ekins.

Performed data analysis: Miller, McGrath, Zorn, Ekins, Wright, Cherrington.

Wrote or contributed to the writing of the manuscript: Miller, McGrath, Zorn, Ekins, Wright, Cherrington.

Acknowledgments

The authors would like to Dr. Ana C. Puhl and Dr. Thomas R. Lane for SARS-CoV-2 discussions. The authors would also like to thank Biovia for providing Discovery Studio used in this study and Alex Clark for software assistance.

References

Bailly C (2021) Pyronaridine: an update of its pharmacological activities and mechanisms of action. *Biopolymers* **112**:e23398.

Baker N, Williams AJ, Tropsha A, and Ekins S (2020) Repurposing quaternary ammonium compounds as potential treatments for COVID-19. *Pharm Res* **37**:104.

Bowes J, Brown AJ, Hamon J, Jarolimek W, Sridhar A, Waldron G, and Whitebread S (2012) Reducing safety-related drug attrition: the use of in vitro pharmacological profiling. *Nat Rev Drug Discov* **11**:909–922.

Clark AM, Dole K, Coulon-Spektor A, McNutt A, Grass G, Freundlich JS, Reynolds RC, and Ekins S (2015) Open source Bayesian models. 1. Application to ADME/Tox and drug discovery datasets. *J Chem Inf Model* **55**:1231–1245.

Clark AM and Ekins S (2015) Open source Bayesian models. 2. Mining a "Big Dataset" to create and validate models with ChEMBL. *J Chem Inf Model* **55**:1246–1260.

Cox RM, Wolf JD, and Plemper RK (2021) Therapeutically administered ribonucleoside analogue MK-4482/EIDD-2801 blocks SARS-CoV-2 transmission in ferrets. *Nat Microbiol* **6**:11–18.

Deen GF, Broutet N, Xu W, Knust B, Sesay FR, McDonald SLR, Ervin E, Marrinan JE, Gaillard P, Habib N, et al. (2017) Ebola RNA persistence in semen of Ebola virus disease survivors–final report. *N Engl J Med* **377**:1428–1437.

Eastman RT, Roth JS, Brimacombe KR, Simeonov A, Shen M, Patnaik S, and Hall MD (2020) Remdesivir: a review of its discovery and development leading to emergency use authorization for treatment of COVID-19. *ACS Cent Sci* **6**:672–683.

Ekins S, Lane TR, and Madrid PB (2020) Tilorone: a broad-spectrum antiviral invented in the USA and commercialized in Russia and beyond. *Pharm Res* **37**:71.

Ekins S, Lingerfelt MA, Comer JE, Freiberg AN, Mirsalis JC, O'Loughlin K, Harutyunyan A, McFarlane C, Green CE, and Madrid PB (2018) Efficacy of tilorone dihydrochloride against Ebola virus infection. *Antimicrob Agents Chemother* **62**:e01711–e01717.

Ekins S and Madrid PB (2020) Tilorone, a broad-spectrum antiviral for emerging viruses. *Antimicrob Agents Chemother* **64**:e00440–e00420.

Ekins S, Puhl AC, Zorn KM, Lane TR, Russo DP, Klein JJ, Hickey AJ, and Clark AM (2019) Exploiting machine learning for end-to-end drug discovery and development. *Nat Mater* **18**:435–441.

Gilead Sciences I (2020) Veklury (remdesivir) [package insert]. U.S. Food and Drug Administration. https://www.accessdata.fda.gov/drugsatfda_docs/label/2020/214787Orig1s000lbl.pdf Accessed [April 20, 2021).

Hofer H, Donnerer J, Sator K, Staufer K, Scherzer TM, Dejaco C, Sator M, Kessler H, and Ferenci P (2010) Seminal fluid ribavirin level and functional semen parameters in patients with chronic hepatitis C on antiviral combination therapy. *J Hepatol* **52**:812–816.

Houzet L, Matusali G, and Dejucq-Rainsford N (2014) Origins of HIV-infected leukocytes and virions in semen. *J Infect Dis* **210** (Suppl 3):S622–S630.

Humeniuk R, Mathias A, Kirby BJ, Lutz JD, Cao H, Osinusi A, Babusis D, Porter D, Wei X, Ling J, et al. (2021) Pharmacokinetic, pharmacodynamic, and drug-interaction profile of Remdesivir, a SARS-CoV-2 replication inhibitor. *Clin Pharmacokinet* **60**:569–583.

Jorgensen SCJ, Kebriaei R, and Dresser LD (2020) Remdesivir: review of pharmacology, pre-clinical data, and emerging clinical experience for COVID-19. *Pharmacotherapy* **40**:659–671.

Kaplon H and Reichert JM (2021) Antibodies to watch in 2021. *MAbs* **13**:1860476.

Klein DM, Evans KK, Hardwick RN, Dantzler WH, Wright SH, and Cherrington NJ (2013) Basolateral uptake of nucleosides by Sertoli cells is mediated primarily by equilibrative nucleoside transporter 1. *J Pharmacol Exp Ther* **346**:121–129.

Kola I and Landis J (2004) Can the pharmaceutical industry reduce attrition rates? *Nat Rev Drug Discov* **3**:711–715.

Lane TR, Dyall J, Mercer L, Goodin C, Foil DH, Zhou H, Postnikova E, Liang JY, Holbrook MR, Madrid PB, et al. (2020a) Repurposing Pyramax®, quinacrine and tilorone as treatments for Ebola virus disease. *Antiviral Res* **182**:104908.

Lane TR and Ekins S (2020) Toward the target: tilorone, quinacrine, and pyronaridine bind to Ebola virus glycoprotein. *ACS Med Chem Lett* **11**:1653–1658.

Lane TR, Massey C, Comer JE, Anantpadma M, Freundlich JS, Davey RA, Madrid PB, and Ekins S (2019) Repurposing the antimalarial pyronaridine tetraphosphate to protect against Ebola virus infection. *PLoS Negl Trop Dis* **13**:e0007890.

Lane TR, Massey C, Comer JE, Freiberg AN, Zhou H, Dyall J, Holbrook MR, Anantpadma M, Davey RA, Madrid PB, et al. (2020b) Pyronaridine tetraphosphate efficacy against Ebola virus infection in guinea pig. *Antiviral Res* **181**:104863.

Li D, Jin M, Bao P, Zhao W, and Zhang S (2020) Clinical characteristics and results of semen tests among men with Coronavirus Disease 2019. *JAMA Netw Open* **3**:e208292.

Lowe SH, van Leeuwen E, Droste JAH, van der Veen F, Reiss P, Lange JMA, Burger DM, Repping S, and Prins JM (2007) Semen quality and drug concentrations in seminal plasma of patients using a didanosine or didanosine plus tenofovir containing antiretroviral regimen. *Ther Drug Monit* **29**:566–570.

Malvy D, McElroy AK, de Clerck H, Günther S, and van Griensven J (2019) Ebola virus disease. *Lancet* **393**:936–948.

Markham A (2021) REGN-EB3: first approval. *Drugs* **81**:175–178.

Miller SR and Cherrington NJ (2018) Transepithelial transport across the blood-testis barrier. *Reproduction* **156**:R187–R194.

Miller SR, Lane TR, Zorn KM, Ekins S, Wright SH, and Cherrington NJ (2021a) Multiple computational approaches for predicting drug interactions with human equilibrative nucleoside transporter 1. *Drug Metab Dispos* **49**:479–489.

Miller SR, Zhang X, Hau RK, Jilek JL, Jennings EQ, Galligan JJ, Foil DH, Zorn KM, Ekins S, Wright SH, et al. (2021b) Predicting drug interactions with human equilibrative nucleoside transporters 1 and 2 using functional knockout cell lines and Bayesian modeling. *Mol Pharmacol* **99**:147–162.

Molina-Arcas M, Casado FJ, and Pastor-Anglada M (2009) Nucleoside transporter proteins. *Curr Vasc Pharmacol* **7**:426–434.

Mruk DD and Cheng CY (2015) The mammalian blood-testis barrier: its biology and regulation. *Endocr Rev* **36**:564–591.

Mruk DD, Su L, and Cheng CY (2011) Emerging role for drug transporters at the blood-testis barrier. *Trends Pharmacol Sci* **32**:99–106.

Mulangu S, Dodd LE, Davey Jr RT, Tshiani Mbaya O, Proschan M, Mukadi D, Lusakibanza Manzo M, Nzolo D, Tshomba Oloma A, Ibanda A, et al.; PALM Writing Group; PALM Consortium Study Team (2019) A randomized, controlled trial of Ebola virus disease therapeutics. *N Engl J Med* **381**:2293–2303.

Naghipour S, Ghodousi M, Rahsepar S, and Elyasi S (2020) Repurposing of well-known medications as antivirals: hydroxychloroquine and chloroquine – from HIV-1 infection to COVID-19. *Expert Rev Anti Infect Ther* **18**:1119–1133.

National Library of Medicine National Clinical Trial (May 2020) (U.S.) The Safety of Molnupiravir (EIDD-2801) and Its Effect on Viral Shedding of SARS-CoV-2 (END-COVID). https://clinicaltrials.gov/ct2/show/NCT04405739

Nies AT, König J, Hofmann U, Kölz C, Fromm MF, and Schwab M (2021) Interaction of remdesivir with clinically relevant hepatic drug uptake transporters. *Pharmaceutics* **13**:369.

Painter WP, Holman W, Bush JA, Almazedi F, Malik H, Eraut NCJE, Morin MJ, Szewczyk LJ, and Painter GR (2021) Human safety, tolerability, and pharmacokinetics of molnupiravir, a novel broad-spectrum oral antiviral agent with activity against SARS-CoV-2. *Antimicrob Agents Chemother* **65**:e02428–e02420.

Pennycooke M, Chaudary N, Shuralyova I, Zhang Y, and Coe IR (2001) Differential expression of human nucleoside transporters in normal and tumor tissue. *Biochem Biophys Res Commun* **280**:951–959.

Politch JA, Mayer KH, Welles SL, O'Brien WX, Xu C, Bowman FP, and Anderson DJ (2012) Highly active antiretroviral therapy does not completely suppress HIV in semen of sexually active HIV-infected men who have sex with men. *AIDS* **26**:1535–1543.

Puhl AC, Fritch EJ, Lane TR, Tse LV, Yount BL, Sacramento CQ, Fintelman-Rodrigues N, Tavella TA, Maranhão Costa FT, Weston S, et al. (2021) Repurposing the Ebola and Marburg virus inhibitors tilorone, quinacrine, and pyronaridine: in vitro activity against SARS-CoV-2 and potential mechanisms. *ACS Omega* **6**:7454–7468.

Robinson CL, Chong ACN, Ashbrook AW, Jeng G, Jin J, Chen H, Tang EI, Martin LA, Kim RS, Kenyon RM, et al. (2018) Male germ cells support long-term propagation of Zika virus. *Nat Commun* **9**:2090.

Sagara I, Beavogui AH, Zongo I, Soulama I, Borghini-Fuhrer I, Fofana B, Traore A, Diallo N, Diakite H, Togo AH, et al.; West African Network for Clinical Trials of Antimalarial Drugs (WANECAM) (2018) Pyronaridine-artesunate or dihydroartemisinin-piperaquine versus current first-line therapies for repeated treatment of uncomplicated malaria: a randomised, multicentre, open-label, longitudinal, controlled, phase 3b/4 trial. *Lancet* **391**:1378–1390.

Sandoval PJ, Zorn KM, Clark AM, Ekins S, and Wright SH (2018) Assessment of substrate-dependent ligand interactions at the organic cation transporter OCT2 using six model substrates. *Mol Pharmacol* **94**:1057–1068.

Siegel D, Hui HC, Doerffler E, Clarke MO, Chun K, Zhang L, Neville S, Carra E, Lew W, Ross B, et al. (2017) Discovery and synthesis of a phosphoramidate prodrug of a Pyrrolo[2,1-f][triazin-4-amino] adenine C-nucleoside (GS-5734) for the treatment of Ebola and emerging viruses. *J Med Chem* **60**:1648–1661.

Soka MJ, Choi MJ, Baller A, White S, Rogers E, Purpura LJ, Mahmoud N, Wasunna C, Massaquoi M, Abad N, et al. (2016) Prevention of sexual transmission of Ebola in Liberia through a national semen testing and counselling programme for survivors: an analysis of Ebola virus RNA results and behavioural data. *Lancet Glob Health* **4**:e736–e743.

Telbisz Á, Ambrus C, Mózner O, Szabó E, Várady G, Bakos É, Sarkadi B, and Özvegy-Laczka C (2021) Interactions of potential anti-COVID-19 compounds with multispecific ABC and OATP drug transporters. *Pharmaceutics* **13**:81.

U.S. Department of Health and Human Services (2020) In Vitro Drug Interaction Studies—Cytochrome P450 Enzyme- and Transporter-Mediated Drug Interactions Guidance for Industry. *Docket Number: FDA-2017-D-5961*. https://www.fda.gov/regulatory-information/search-fda-guidance-documents/vitro-drug-interaction-studies-cytochrome-p450-enzyme-and-transporter-mediated-drug-interactions

Uyeki TM, Erickson BR, Brown S, McElroy AK, Cannon D, Gibbons A, Sealy T, Kainulainen MH, Schuh AJ, Kraft CS, et al. (2016) Ebola virus persistence in semen of male survivors. *Clin Infect Dis* **62**:1552–1555.

Wahl A, Gralinski LE, Johnson CE, Yao W, Kovarova M, Dinnon 3rd KH, Liu H, Madden VJ, Krzystek HM, De C, et al. (2021) SARS-CoV-2 infection is effectively treated and prevented by EIDD-2801. *Nature* **591**:451–457.

Address correspondence to: Nathan J. Cherrington, 1703 E. Mabel St, Tucson, Arizona 85721. E-mail: cherrington@pharmacy.arizona.edu